

Structure–Selectivity Investigations of D₂-Like Receptor Ligands by CoMFA and CoMSIA Guiding the Discovery of D₃ Selective PET Radioligands

Ismail Salama,[†] Carsten Hocke,[‡] Wolfgang Utz,[†] Olaf Prante,[‡] Frank Boeckler,[†] Harald Hübner,[†] Torsten Kuwert,[‡] and Peter Gmeiner^{*†}

Department of Medicinal Chemistry, Emil Fischer Center, Friedrich Alexander University, Schuhstrasse 19, D-91052 Erlangen, Germany, and Department of Nuclear Medicine, Krankenhausstrasse 12, D-91054 Erlangen, Germany

Received September 26, 2006

Elucidation of the physiological role of the D₃ receptor and its distribution in the brain using positron emission tomography (PET) is hampered by the lack of bioavailable subtype selective tracer ligands. To develop appropriate D₃ radioligands, we designed an integrative procedure involving the elucidation of structural features determining D₃ selectivity over both congeners D₂ and D₄ by comparative molecular analysis. Thus, we have successfully generated CoMFA and CoMSIA models based on the affinity differences of a series of 79 ligands representing a broad range of selectivities. These models yielded highly significant cross-validations ($q^2_{cv}(D_3/D_2) = 0.86$; $q^2_{cv}(D_3/D_4) = 0.92$) and excellent predictions of a 16-ligand test set ($r^2_{pred} = 0.79–0.93$). Exploiting this information, synthesis and receptor binding studies directed us to the fluorinated lead compounds **78** and **79**, featuring subnanomolar D₃ affinities and considerable selectivities over D₂ and D₄ and, subsequently, to the subtype selective PET tracers [¹⁸F]**78** and [¹⁸F]**79**.

Introduction

Positron emission tomography (PET^a) is a high-performance molecular imaging technology that allows for functional and quantitative information on receptor densities in the CNS.¹ PET has already gained growing importance for the diagnosis of Morbus Parkinson by *in vivo* imaging of alterations of the dopaminergic signaling pathways and disturbances of D₂-like receptor densities using the radiopharmaceuticals 6-[¹⁸F]fluoro-L-dopa² and [¹¹C]raclopride,³ respectively. More recently, the availability of the D₂ and D₃ binding radioligand [¹⁸F]fallypride enabled PET studies on human beings for the exploration of low D₂/D₃ receptor densities in the cortex besides higher levels in the putamen.⁴

The lack of bioavailable D₃-subtype selective PET ligands excluding crosstalk with the strongly related subtypes D₂ and D₄ still hampers a noninvasive investigation of the physiological role of D₃. Because the D₃ receptor is an interesting therapeutic target for the treatment of Parkinson's disease and schizophrenia,⁵ this method would probably guide us to a better understanding of the genesis and the therapy of these disorders.

In the past, various attempts have been made to develop a suitable PET ligand for the dopamine D₃ receptor including the preparation of the ¹¹C-labeled imidazo[2,1-*b*]thiazolylpiperazine derivative RGH-1756 and the substituted aminotetraline [¹¹C]GR218231.^{6–8} Using the benzothiophene derivative **7** (FAUC 365) as a lead compound,⁹ we synthesized fluorine-18-labeled derivatives as putative PET imaging agents.¹⁰ However, the above-mentioned tracers showed a low signal for specific binding to the D₃ receptor or rapid efflux from the brain *in vivo*

and disappointing binding characteristics in preliminary autoradiography experiments. Thus, the discovery of highly selective radioligands as PET tracers is still an important aim announcing new insights into the role of the D₃ receptor subtype in the pathophysiology of numerous diseases.

To efficiently approach suitable D₃ radioligands, we expected an integrative procedure involving the elucidation of structural features determining D₃ selectivity by comparative molecular analysis to be highly beneficial. Extending our recent work on the 3D-QSAR (3D-quantitative structure–activity relationship) analyses of dopaminergic agents,^{11–13} we herein describe the generation of selectivity contour maps by CoMFA and comparative molecular similarity indices analysis (CoMSIA)^{14–23} displaying the molecular origins for a subtype specific recognition of D₃ over both congeners D₂ and D₄.^{24–35} Exploiting this information, the synthesis and receptor binding studies of fluorinated lead compounds led us to the selective PET tracers [¹⁸F]**78** and [¹⁸F]**79**.

Results and Discussions

Assembly of the Training Set. Taking advantage of our in-house data on D₂-like ligands,^{10,36–42} we created a training set of 63 structurally diverse compounds all belonging to the privileged structure of 1,4-disubstituted arylpiperidines and -piperazines. The training set was assembled from class A, B, and C compounds representing D₃- and D₄-selective ligands and D₂ preferential ligands, respectively (Chart 1). A vital part of our modeling strategy was to enrich our training set of our in-house dopaminergics **2–46** and **50–63** by a number of external reference ligands, including **1** (BP 897),⁴³ **47** (L-745,870),⁴⁴ **48** (haloperidol), and **49** (aripiprazole), thus enhancing the ligands' structural diversity. To ensure that the experimentally obtained D₃/D₂ and D₃/D₄ affinity differences are the result of consistent assay conditions, all biological data have been measured in our lab.

Alignment. Finding a suitable alignment is probably the most important step to establish a 3D-QSAR model successfully. This was even more crucial for our bidirectional quantitative structure–selectivity relationship (QSSR) model that was

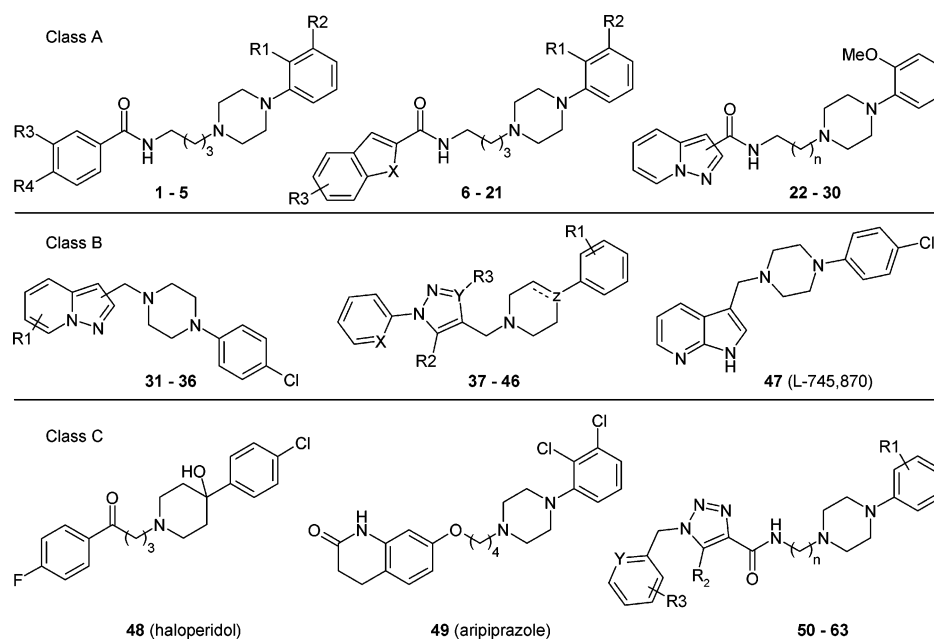
* To whom correspondence should be addressed. Tel.: +49 (9131)-8529383. Fax: +49(9131)-8522585. E-mail: gmeiner@pharmazie.uni-erlangen.de.

[†] Department of Medicinal Chemistry.

[‡] Department of Nuclear Medicine.

^a Abbreviations: PET, positron emission tomography; QSAR, quantitative structure–activity relationship; CoMSIA, comparative molecular similarity indices analysis; QSSR, quantitative structure–selectivity relationship; PLS, partial least-squares; APS, all placement search; AOS, all orientation search.

Chart 1



expected to precisely predict D_3 selectivity over both congeners D_2 and D_4 . After compiling representative conformations and deducing the shape of all other ligands thereof, we decided to employ one common alignment for both QSSR models when the D_3 -selective antagonist **7** was selected as a template. The alignment was performed by comparison of steric overlap and molecular electrostatic potentials using the module ASP,⁴⁵ as implemented in the program package TSAR⁴⁶

CoMFA. The CoMFA method was employed for deriving a 3D-QSSR model consisting of a training set of 63 ligands (Chart 1, Table 1). The leave-one-out partial least-squares (PLS) analysis of the obtained models yielded excellent cross-validated q^2 -values of 0.85 (four components) and 0.92 (five components) for D_3/D_2 and D_3/D_4 selectivity, respectively. These correlation coefficients suggest that our model is reliable and accurate. Subsequently, non-cross-validated PLS regressions were computed using the previously obtained optimum number of components giving regression coefficients r^2 of 0.95 (D_3/D_2) and 0.98 (D_3/D_4) (Table 2). To quantify the translational dependence of q^2 , we applied the all placement search (APS) procedure published by Wang et al.,⁴⁷ which systematically translates the aligned dataset in space. Starting from the default region, the upper and lower margins are systematically increased by increments of 0.1 Å in the direction of the x , y , and z axes until the grid spacing distance of 1.0 Å is reached. By this translation process, we obtained $10 \times 10 \times 10 = 1000$ different placements, followed by PLS analysis after every retranslation. Figure 1 shows the frequency distribution of the obtained q^2 values among all the placements after the translation (1 Å lattice). The range of the values 0.84–0.88 (D_3/D_2) and 0.91–0.93 (D_3/D_4) is quite narrow, indicating that our CoMFA model is rather stable toward different grid placements. The highest q^2 for (D_3/D_2) 0.88 was found for 10 components with $s_{c/v} = 0.50$, while for (D_3/D_4), the highest q^2 was 0.93 for 10 components with $s_{c/v} = 0.63$. However, it should be noted that, frequently, an increase of $q^2_{c/v}$ values by less than 5% for the use of an additional component is considered inappropriate due to the “parsimony principle”.⁴⁸ Thus, we used the original models, which are in line with this rule, to derive the graphical CoMFA maps. During the optimization of our CoMFA model, variations of parameters, such as grid spacing and cutoff values

for steric/electrostatic energies, did not improve the model. The step by step modification of these parameters was done manually (we did not use a respective algorithm).

For the grid spacing, we used a 1 Å lattice although this increased the computation time by a factor of 8 (compared to the default value of 2.0 Å) trying to ensure that no important contributions to the correlation analysis were lost due to the arbitrary cutoff values.¹⁹

CoMSIA. CoMSIA computes the steric and electrostatic fields (as in CoMFA), but it also calculates additional hydrophobic, hydrogen-bond donor, and hydrogen-bond acceptor fields. The resulting contour maps are easier to interpret than those in CoMFA because a Gaussian function is used to determine the distance-dependence. Therefore, the similarity indices can also be calculated at the grid points inside the molecules, not just outside, as it is in CoMFA.¹⁵

Several CoMSIA models were generated using the combinations of different fields (Table 2). The purpose of using several combinations of different fields is not only to increase the significance and predictive power of the 3D-QSSR models, but also to partition the various properties into spatial locations where they play a decisive role in determining the selectivity. CoMSIA, in most instances, performs similarly to CoMFA in terms of predictive ability. The results of the initial CoMSIA models for different combinations are summarized in Table 2. For D_3/D_2 selectivity CoMSIA runs, q^2 values of over 0.86 were obtained, indicating that the obtained models should be more accurate than the corresponding CoMFA models in predicting the D_3/D_2 selectivity values, while for D_3/D_4 selectivity, the CoMFA model performs significantly better than CoMSIA models based on the obtained q^2 and r^2 values. For D_3/D_2 selectivity, a combined use of all the five descriptors resulted in the best model ($q^2 = 0.86$ and $r^2 = 0.94$ with four components). For D_3/D_4 selectivity, a combined use of the steric, electrostatic, hydrophobic, and hydrogen-bond donor descriptors produced the best model ($q^2 = 0.91$ and $r^2 = 0.97$ with four components).

Validation of the QSSR Models. Employing a test set of 14 ligands, we intended to verify the excellent statistical parameters that we observed and to investigate whether fluorine-substituted derivatives can be predicted well. As can be seen in

Table 1. Data Set of 63 Compounds Used in the Training Set and Their Experimental and Predicted Selectivity^a

cpd	pos	n	X	Y	Z	R ₁	R ₂	R ₃	R ₄	D ₃ /D ₂ (exp)	ΔD ₃ /D ₂ ^e		D ₃ /D ₄ (exp)	ΔD ₃ /D ₄ ^e	
											CoMFA	CoMSIA		CoMFA	CoMSIA
1						OMe	H	–(CH) ₄ –		2.17	–0.15	–0.01	1.44	–0.13	–0.34
2						Cl	H	–(CH) ₄ –		2.66	0.10	0.05	2.30	–0.07	–0.50
3						Cl	H	H	Cl	2.44	0.28	0.12	2.22	0.79	0.61
4						Cl	H	OMe	OMe	1.96	–0.37	–0.29	1.74	–0.56	–0.44
5						Cl	H	H	Ph	2.66	–0.51	–0.02	2.93	–0.17	–0.15
6 ^b			S			OMe	H	H		2.57	0.21	0.50	1.81	0.32	0.61
7			S			Cl	Cl	H		3.86	0.66	1.07	2.83	–0.05	0.19
8			S			OMe	H	5CCH		3.02	0.75	1.01	1.90	0.12	0.36
9			S			OMe	H	5-CN		2.17	–0.40	0.10	1.99	0.13	0.52
10			S			OMe	H	6CCH		2.72	0.46	0.74	2.60	0.93	1.10
11			O			OMe	H	H		1.99	–0.03	–0.08	1.43	0.20	0.25
12			O			Cl	Cl	H		2.43	–0.59	–0.60	1.89	–0.62	–0.65
13			O			OMe	H	5-Br		2.14	–0.19	–0.31	1.39	–0.36	–0.51
14			O			Cl	Cl	5-Br		3.46	0.53	0.40	2.95	0.38	0.45
15			O			OMe	H	5-CN		1.48	–0.78	–0.63	1.13	–0.40	–0.27
16			N			Cl	Cl	H		3.67	0.48	0.30	3.41	0.55	0.44
17			N			OMe	H	5-CN		2.39	0.10	–0.17	1.62	–0.13	–0.12
18			N			OMe	H	5-Br		2.65	0.29	–0.22	1.81	0.02	–0.12
19			N			OMe	H	6-CN		2.80	0.54	0.44	2.20	0.39	0.39
20			N			Cl	Cl	5-Br		3.49	0.14	–0.22	2.91	–0.18	–0.46
21			N			Cl	Cl	6-CN		2.98	–0.29	–0.37	3.25	0.01	0.16
22	2	1								0.32	0.25	0.66	–0.92	1.27	1.15
23	2	2								0.11	0.31	0.72	–1.20	0.28	0.19
24	2	3								1.86	–0.39	0.30	1.48	0.04	0.02
25	2	4								0.14	–0.07	0.48	0.18	–0.41	–0.63
26	3	1								–0.10	–0.71	–0.57	–2.73	–1.99	–2.28
27	3	4								–0.33	0.07	0.17	0.02	0.40	0.42
28	4	3								1.13	0.06	–0.55	0.64	0.06	–0.27
29	5	3								1.83	–0.15	0.33	1.38	0.19	0.46
30	7	3								0.72	–0.58	–1.07	–0.51	–1.07	–1.16
31 ^c	3					H				–0.14	–0.40	–0.23	–3.23	0.82	0.33
32	3					6-CH ₂ OH				1.03	0.88	0.14	–2.12	–0.41	0.21
33	3					7-I				0.45	0.34	0.75	–2.73	1.03	1.01
34	3					7-CH ₃				0.12	–0.38	–0.20	–3.14	–0.34	–0.44
35	3					7-CCH				–0.09	–0.42	–0.21	–3.57	–0.28	0.00
36 ^d	2					H				–0.19	–0.23	0.12	–3.38	–1.46	–0.57
37			N	C	N	H	H	H		0.33	0.63	0.33	–1.79	0.65	0.40
38			N	C	N	2-OMe	H	H		–0.26	–0.15	–0.25	–2.22	–0.35	–0.05
39			C	C	N	H	H	H		0.00	–0.24	–0.05	–2.15	0.53	0.03
40			C	C	N	4-Cl	H	H		0.18	0.11	–0.07	–2.82	–0.95	–1.03
41			C	C	N	4-F	H	H		–0.08	0.06	0.04	–2.72	0.11	0.00
42			C	C	N	2-F	H	H		–0.03	0.00	–0.21	–1.98	0.31	0.08
43			C	C	N	H	H	CH ₃		–0.71	–0.69	–0.94	–2.56	0.19	–0.45
44			C	C	N	H	CH ₃	H		0.29	0.21	0.44	–1.79	0.05	0.54
45			C	C	C	H	H	H		0.06	–0.25	0.03	–1.75	–0.33	–0.36
46			C	N	C	H	H	H		0.37	0.47	0.35	–1.46	0.53	0.31
47										0.24	0.08	–0.14	–4.70	–1.47	–1.39
48										–0.87	–1.71	–1.13	–0.14	–0.28	0.66
49										–0.39	–1.94	–1.17	1.11	–0.16	1.02
50	4					2,3-diCl	CH ₃	H		0.96	0.01	–0.46	1.82	0.36	–0.29
51	4					2-OCH ₃	CH ₃	H		0.53	–0.11	–0.15	1.16	–0.19	–0.04
52	5					2,3-diCl	CH ₃	H		0.07	0.82	0.45	1.47	0.71	0.65
53	5					2-Ome	CH ₃	H		–0.23	0.21	0.32	1.00	0.60	0.90
54	4					2,3-diCl	<i>n</i> -propyl	H		0.77	–0.11	–0.36	1.96	0.58	0.34
55	4					2-Ome	<i>n</i> -propyl	H		0.72	0.34	0.39	1.44	0.23	0.60
56	4					2-Ome	CH ₃	4-Ome		0.28	0.00	–0.48	0.99	0.13	–0.28
57	5					2,3-diCl	CH ₃	4-Ome		–0.57	–0.38	–0.47	0.93	–0.21	0.48
58	5					2-Ome	CH ₃	4-Ome		–0.71	–0.84	–0.42	0.49	–0.74	–0.23
59	4					2-Ome	<i>n</i> -propyl	4-Ome		0.52	0.10	–0.10	1.00	–0.10	–0.15
60	4					2-Ome	CH ₃	2-Br		0.28	–0.31	–0.54	0.45	–0.55	–0.76
61	5					2-Ome	CH ₃	2-Br		–0.49	–0.33	–0.36	0.44	–0.30	–0.32
62	4					2-Ome	<i>n</i> -propyl	2-Br		0.80	0.41	0.37	1.34	0.39	0.50
63	5					2-Ome	<i>n</i> -propyl	2-Br		–0.15	0.17	0.28	0.73	–0.04	–0.25

^a Calculated as $-\log(K_i(D_3)/K_i(D_2))$ and $-\log(K_i(D_3)/K_i(D_4))$, respectively. ^b FAUC 346.³⁹ ^c FAUC 113.³⁶ ^d FAUC 213.³⁷ ^e $\Delta(D_3/D_2)/(D_3/D_4)$ is the error of fitted selectivities = $[(D_3/D_2)/(D_3/D_4)_{\text{experimental}} - (D_3/D_2)/(D_3/D_4)_{\text{fitted}}]$.

Table 2, the trained CoMFA and CoMSIA models can reproduce the experimental data very well for both D₃/D₂ and D₃/D₄ selectivity values of all the compounds included in the training set. The ultimate test for the predictability of a QSAR or a QSSR analysis in the drug design process is to predict the biological activity/selectivity of new compounds that have not been

included in the training set. The 3D-QSSR models obtained in this study were challenged with a test set consisting of 14 randomly selected compounds (**64**–**77**, Table 3) from the original dataset of 77 ligands. The predicted versus the experimental selectivity values for the training set, the test set, and two newly synthesized compounds (**78** and **79**) are depicted

Table 2. Summary of the 3D-QSSR Models^a

PLS statistic	D3/D2 model				D3/D4 model			
	CoMFA	CoMSIA			CoMFA	CoMSIA		
	SE	SEHDA	SEHD	SED	SE	SEHDA	SEHD	SED
q^2_{cv}	0.85	0.86	0.86	0.86	0.92	0.90	0.91	0.90
s_{PRESS}	0.53	0.51	0.51	0.51	0.62	0.62	0.64	0.66
r^2	0.95	0.94	0.94	0.93	0.98	0.97	0.97	0.96
S	0.29	0.33	0.33	0.35	0.30	0.39	0.39	0.40
F	300.0	227.9	232.5	203.8	565.2	428.7	426.6	391.0
components	4	4	4	4	5	4	4	4
descriptors	3544	6581	5609	3525	3544	6581	5609	3525
field contribution								
steric	0.639	0.062	0.094	0.166	0.666	0.121	0.148	0.222
electrostatic	0.361	0.184	0.251	0.434	0.334	0.202	0.255	0.449
hydrophobic		0.283	0.388			0.271	0.341	
donor		0.195	0.267	0.400		0.215	0.256	0.329
acceptor		0.276				0.190		

^a S, steric; E, electrostatic; H, hydrophobic; D, donor; A, acceptor.

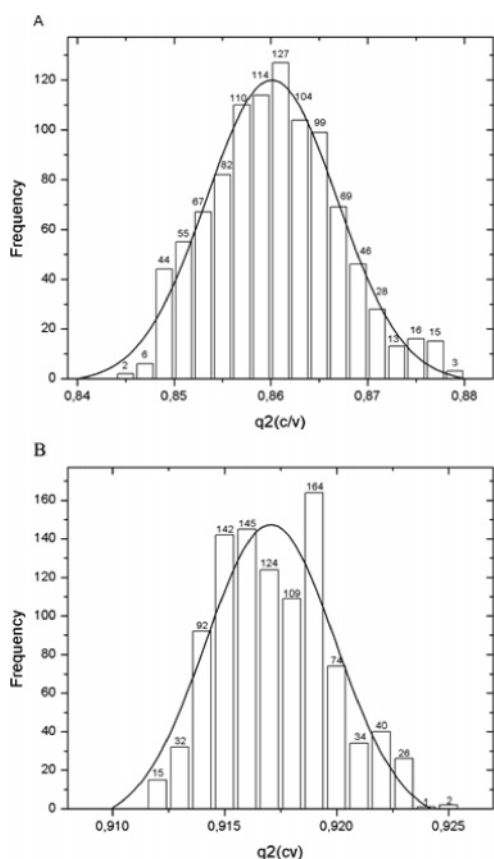


Figure 1. Histogram showing the distribution of q^2 values calculated by SAMPLS leave-one-out cross-validation of D₃/D₂ selectivity CoMFA (A) and D₃/D₄ selectivity CoMFA (B) after systematic translation of aligned molecules within the lattice by an APS.

in Figure 2. In addition to these test set ligands, we also included **78** and **79** in the calculation of the r^2_{pred} value. The calculation was performed according to the formula of Cramer et al.¹⁴ and gave better results for CoMFA, with $r^2_{pred} = 0.84$ than for the CoMSIA model ($r^2_{pred} = 0.78$) in the case of D₃/D₂ selectivity. The r^2_{pred} of the D₃/D₄ selectivity showed values of 0.90 and 0.93 for CoMFA and CoMSIA models, respectively. Thus, our models display very high predictivity both in regular cross-validation and in the prediction of a test set. For a rational design of [¹⁸F]-labeled PET ligands, it was of special interest for us to see that the calculated D₃/D₂ and D₃/D₄ selectivities of the fluorinated test compounds **74**–**77** proved to be in good accordance to the experimentally derived affinity differences.

3D Contour Maps. To visualize the information content of the derived 3D-QSSR models, CoMFA and CoMSIA contour maps were generated. The field energies at each lattice point were calculated as the scalar results of the coefficient and the standard deviation associated with a particular column of the data table (“stdev*coeff”), which was always plotted as the percentage of the contribution to the CoMFA or CoMSIA equation. In the figures discussed below, the isocontour diagrams of the field contributions (“stdev*coeff”) for different properties calculated by the CoMFA and CoMSIA analysis are illustrated with exemplary ligands. Selectivity fields depict the change in binding preference occurring upon the change in molecular fields around ligands. The contour plots may help to identify important regions where any change may affect the binding preference. Furthermore, they may be helpful in identifying important features contributing to interactions between the ligand and the active site of a receptor.

Models for D₃/D₂ Selectivity. In Figure 3, panels A and B, the steric properties derived from the D₃/D₂ selectivity data are displayed for CoMSIA. Areas indicated by green contours correspond to regions where steric occupancy with bulky groups should increase selectivity of D₃ against D₂. Areas encompassed by yellow isopleths should be sterically avoided; otherwise, reduced D₃/D₂ selectivity can be expected. As depicted, the cyanoindeole derivative **21**, a very D₃-selective ligand, orients its heterocyclic ring to a green area, while the very low D₃/D₂-selectivity of the 3-substituted azaindeole **27** could be due to the orientation of its pyrazolopyridine system to a yellow region. Accordingly, the methyl groups of **50**, **51**, **57**, and **60** and the propyl group of **55**, **59**, and **62** are pointing toward the lower yellow area. The triazole moieties of **50**–**63** are directed to the upper, unfavored yellow isopleth. In addition, the yellow map near the *ortho*-position of the phenyl group indicates that bulky substituents there may decrease the D₃/D₂ selectivity. This observation is confirmed by the fact that *ortho*-methoxyphenyl containing ligands always display lower selectivity compared to the dichlorophenyl derivatives. In panels C and D, the electrostatic property maps include **16** and **57** as examples for high and low D₃-selectivity ligands, respectively. The blue and red areas above and below the carboxamide moiety of the indolyl-2-carboxamide **16** reflect a common placement of this function within highly selective ligands. The other blue and red areas are positioned in the vicinity of the protonated piperazine nitrogen (N1) and the electron-rich, tertiary nitrogen (N2) of highly selective ligands. Consequently, these two isopleths determine the preferred position of the piperazine ring. In

Table 3. Data set of 16 Compounds Used in the Test Set and Their Experimental and Predicted Selectivities^a

64 - 79

Cpd.	Het(Ar)	X	R ₁	R ₂	D ₃ /D ₂ (exp.)	Δ D ₃ /D ₂ ^e		D ₃ /D ₄ (exp.)	Δ D ₃ /D ₄ ^e	
						CoMFA	CoMSIA		CoMFA	CoMSIA
64 ^b			-OCH ₃	H	0.78	-0.19	-0.34	0.38	-0.30	-0.58
65 ^b			-OCH ₃	H	-1.14	-0.33	-0.67	-1.03	0.24	0.03
66 ^b			-OCH ₃	H	1.52	-0.49	-0.16	0.97	-0.39	-0.01
67			-OCH ₃	H	2.28	-0.31	-0.15	2.35	0.431	0.633
68			-Cl	3-Cl	2.89	-0.38	-0.14	1.77	-1.55	-1.33
69			-Cl	3-Cl	3.21	-0.18	0.37	3.41	0.09	0.62
70			-Cl	3-Cl	2.52	-0.66	-0.36	2.73	0.32	-0.13
71			-Cl	3-Cl	2.85	-0.50	0.01	2.45	-0.71	-0.26
72			H	4-CCH	0.50	0.28	0.55	-3.44	0.38	0.09
73 ^c			-OCH ₃	H	-0.50	-0.42	-0.42	-2.09	0.34	0.06
74 ^d			-OCH ₃	H	1.37	0.44	-0.32	0.90	0.70	0.42
75 ^d			-Cl	3-Cl	1.51	-0.25	-1.04	1.92	0.59	0.11
76 ^d			-OCH ₃	H	1.05	-0.19	-0.67	0.96	0.45	0.40
77 ^d			-Cl	3-Cl	1.28	-0.72	-1.25	1.96	0.39	-0.24
78			-OCH ₃	H	1.86	-0.43	-0.01	1.88	0.02	-0.14
79			-OCH ₃	H	1.53	-0.928	-0.31	1.88	-0.37	-0.07

^a Calculated as $-\log(K_i(D_3)/K_i(D_2))$ and $-\log(K_i(D_3)/K_i(D_4))$, respectively. ^b Reference 39. ^c Reference 42. ^d Reference 10. ^e $\Delta(D_3/D_2)/(D_3/D_4)$ is the error of predicted selectivities = $[(D_3/D_2)/(D_3/D_4)_{\text{experimental}} - (D_3/D_2)/(D_3/D_4)_{\text{predicted}}]$.

contrast, the red area for the benzyltriazole **57** is completely buried in the transparent blue electrostatic potential at the N1, while the transparent red electrostatic potential at the N2 is completely embedded in the blue mesh. The hydrophobic effect on the selectivity can be drawn from panels E and F, suggesting that occupation of the 2 or 2 and 3 positions of the phenyl ring by a hydrophobic group is crucial for a highly selective D₃/D₂ ligand, as illustrated by compounds **7**, **12**, **14**, **16**, **20**, **21**, and

50 and **2**, **3**, **4**, and **5**, respectively, while the yellow mesh on the left is due to the Br of **14** and **20** and the Cl of **3**. The *N*-benzyltriazole carboxamides, which have very reduced D₃/D₂ selectivity, have 2-chloro substituents in the small orange isopleth on the left side, which is exemplified by ligands **60**–**63**.

Models for D₃/D₄ Selectivity. Steric and electrostatic fields of CoMFA contour maps are shown in Figure 4. The presence

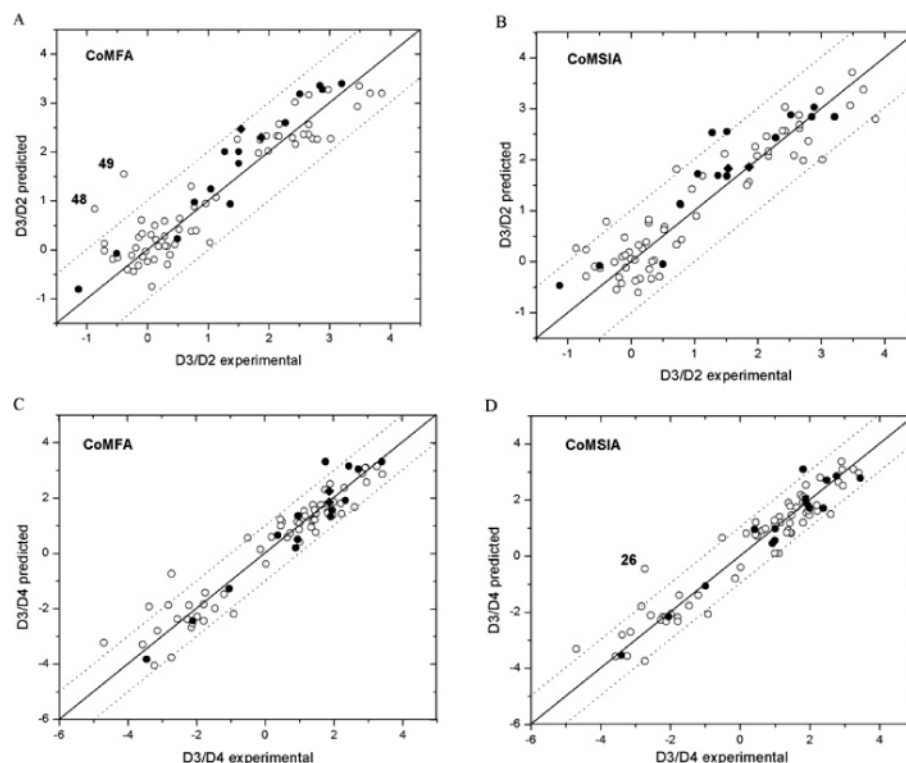


Figure 2. Plots of the predicted versus observed selectivity values. A and C represent CoMFA results, whereas B and D refer to CoMSIA results. Training set compounds (1–63) are indicated by open circles and test set compounds are indicated by filled circles (64–77) or filled rhombi (78–79).

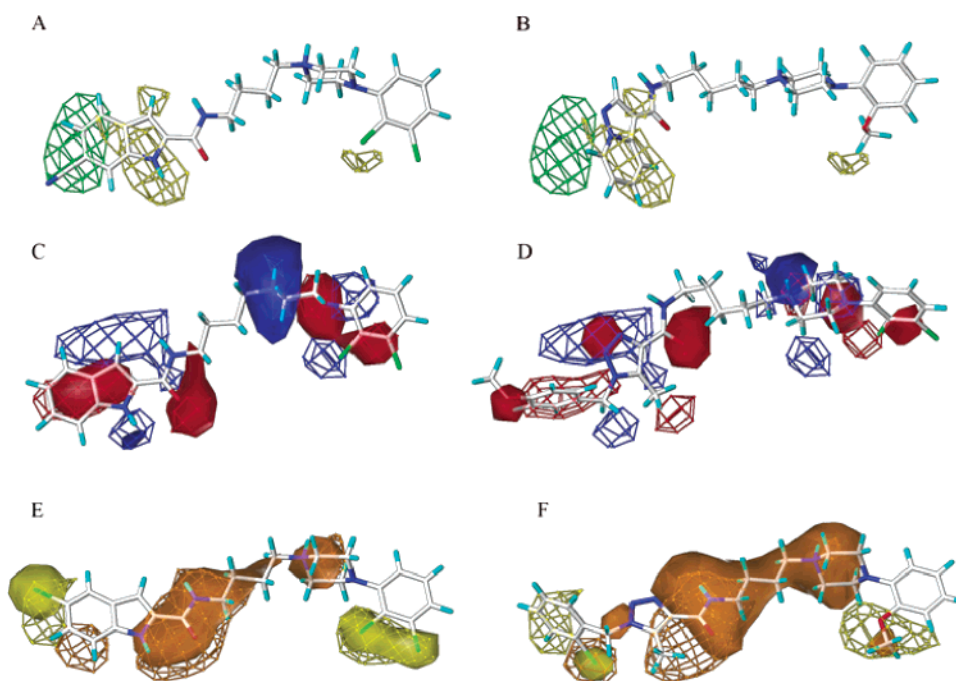


Figure 3. Contour maps of a D_3/D_2 selectivity CoMSIA model illustrating steric (A and B), electrostatic (C and D), and hydrophobic (E and F) properties. For all features, one ligand with high (A, **21**; C, **16**; E, **20**) and another with low D_3/D_2 selectivity (B, **27**; D, **57**; F, **60**) are shown in comparison. The mesh fields represent the $\text{stdev} \times \text{coeff}$ plots, whereas the transparent surfaces indicate the fields of the particular ligand, thus facilitating the recognition of matching or mismatching features. In A and B, green isopleths enclose areas where steric bulk will enhance the selectivity. Yellow contours highlight areas that should be kept unoccupied, otherwise the selectivity will decrease. In C and D, red isopleths enclose areas where an increase of negative charge will enhance selectivity, whereas in blue-contoured areas, an increase of positive charge is favorable for selectivity. In E and F, yellow isopleths encompass regions favorable for hydrophobic groups, and in orange-contoured areas, more hydrophilic groups are favorable for selectivity.

of a substituent near a green region, the absence of a substituent near a yellow region, the increase of a negative charge near a red region, or a positive charge near a blue region shifts the binding preference toward the D_3 receptor, while the presence

of a substituent near a yellow region, the absence of a substituent near a green region, the increase of a negative charge near a blue region, or a positive charge near a red region shifts the binding preference in the opposite direction toward the D_4

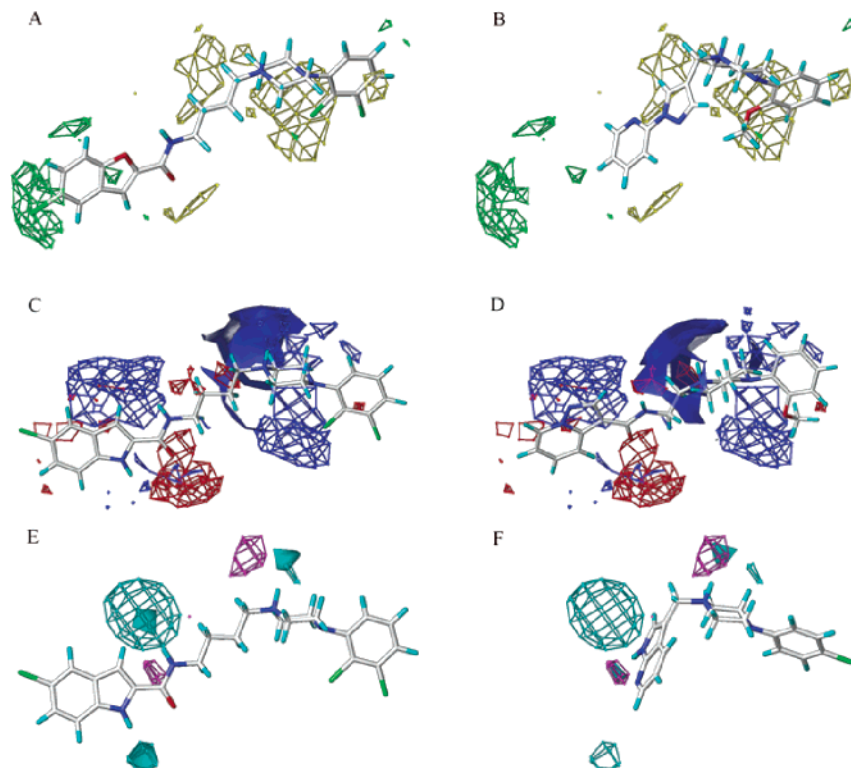


Figure 4. Contour maps of D_3/D_4 selectivity models as obtained by CoMFA (A, B, C, and D) and CoMSIA (E and F) analyses. These maps are demonstrated by the highly selective compounds (A, **14**; C, **20**; E, **20**) and less-selective compounds (B, **38**; D, **26**; F, **4**). In A and B, green isopleths enclose areas where steric bulk will enhance the selectivity. Yellow contours highlight areas that should be kept unoccupied, otherwise the selectivity will decrease. In C and D, red isopleths enclose areas where an increase of negative charge will enhance selectivity, whereas in blue-contoured areas an increase of positive charge is favorable for selectivity. In E and F, isopleths in cyan represent regions of hydrogen-bond acceptors on the receptor site.

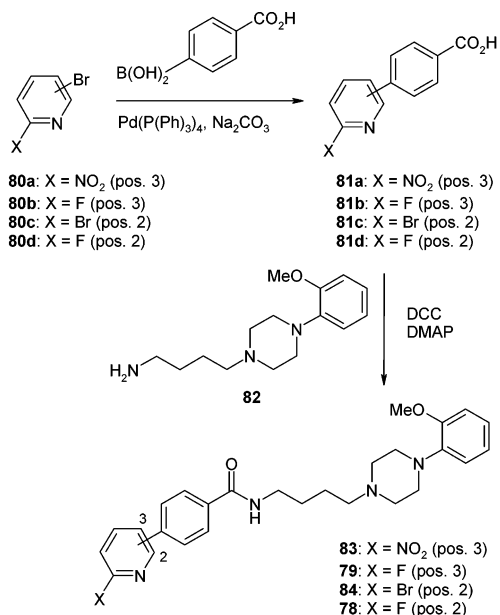
receptor. Such fields could, in principle, suggest the way a leading structure should be modified for gaining higher selectivity. Panels A and B display the benzofurane **14** as an example for a highly selective D_3 ligand, and the pyrazole **38** as an example for a ligand having very low selectivity. The green areas near the benzofurane positions 5, 6, and 7 in **14** indicate that sterically demanding substituents in these positions favor D_3/D_4 selectivity. This is also the case with **8–10**, **13–15**, and **17–21**. The yellow maps positioned on the right side are due to all the biaryl- or heteroarylmethylene derivatives that have very low D_3/D_4 selectivity and a bent orientation determining this V shape of the yellow areas. In panels C and D, the carboxamides **20** and **26** are depicted as examples for highly D_3 -selective and low-selective ligands, respectively. The two blue and red electrostatic isocontours on the left arise from the appropriately positioned carboxamide function of all the highly D_3 -selective ligands, while the blue area above the piperazine ring corresponds to the protonated N1 of those ligands. Because of the lower spacer length of **26**, the piperazine moiety is shifted left placing the protonated N1 and the N2 in the red and blue isopleth, respectively. Furthermore, the two pyrazolopyridine nitrogens as well as the *o*-methoxy substituent are directed to unfavorable large blue areas. So the selectivity for the D_3 receptor is larger for the four-carbon spacer carboxamides, and it is dramatically decreased by decreasing or increasing the number of the C-spacer or removing the carboxamide moiety. The graphical interpretation of the field contributions of the H-bond donor (from CoMSIA) is shown in panels E and F. Cyan isopleth contour maps define where a H-bond donor group within a ligand will be advantageous for the binding preference toward the D_3 receptor, while purple isopleths represent H-bond donors that shift the binding preference in the opposite direction

toward the D_4 receptor. In principle, they should highlight the areas beyond the ligands where putative partners in the receptor can form a hydrogen bond that will influence the binding affinity and selectivity significantly. For the D_3 -selective ligand **20**, the cyan transparent area of the protonated N1 is positioned on the cyan mesh, which corresponds to the Asp3.32 in the D_3 receptor. However, the cyan transparent near N2 of the D_4 -selective azaindole **47** is aligned on the purple mesh.

Prediction of D_3 -Selective PET Tracers. Based on our initial approach toward the development of D_3 radioligands for PET involving the test compounds [^{18}F]-**74–77**,¹⁰ this work focused on the rational prediction of novel [^{18}F]-labeled PET ligands with improved D_3 receptor selectivity. Consequently, we chose the highly potent biphenylcarboxamide **5** ($K_i = 0.28$ nM) as an interesting lead compound for the structural design of potential PET tracers. To decrease the lipophilicity of the target compounds causing accumulation in membranes and, thus, very high unspecific binding (**5**: $\text{ClogP} = 5.94$) and simultaneously gaining the possibility to perform nucleophilic [^{18}F]-substitution reactions using *ortho*-(hetero)aryl halides as labeling precursors, we examined further substitution patterns by replacing phenyl by an *ortho*-fluoro-substituted pyridine nucleus, and also *o*-chlorine by an *o*-methoxy substituent, to obtain the azabiphenyl derivatives **78** and **79**, which can be described as structural hybrids of the lead compound **5** and the fluoropyridylcarboxamides **76/77**. Structurally related biphenyl carboxamides, such as GR 103691 and NGB 2904, have already been described as selective antagonists for D_3 receptors.^{5,49,50}

When the target compounds **78** and **79** were predicted employing the CoMFA and CoMSIA model, the 2-fluoropyridin-6-yl derivative **78** was suggested to have a D_3/D_2 selectivity of 2.29/1.87 and a D_3/D_4 selectivity of 1.86/2.02 as predicted

Scheme 1. Synthetic Pathway of the Predicted D₃ Ligands (**79** and **78**) as References of Their ¹⁸F-Labeled Analogs and the Respective Precursor Compounds **83** and **84**



from CoMFA/CoMSIA, respectively. The 2-fluoropyridin-5-yl derivative **79** was supposed to give a D₃/D₂ selectivity of 2.46/1.84 and a D₃/D₄ selectivity of 2.25/1.95 by CoMFA/CoMSIA prediction, respectively. It is also worthy to note that the calculation of log *P* values indicated a significant loss of lipophilicity due to the C,N exchange (**5**, C log *P* = 5.35; **78**, C log *P* = 3.57; **79**, C log *P* = 3.36).

At this point, we were ready to precede with the synthesis of the two novel ligands **78** and **79** to verify our aforementioned predictions by *in vitro* biological testing and to investigate the radiochemical accessibility of the [¹⁸F]-labeled PET ligands.

Chemistry and Radiolabeling. After verifying that D₃ selectivities of fluorine-substituted test compounds can be predicted well, we tried to prove the effectiveness of the new QSSR models in the design and synthesis of novel D₃-selective PET ligands. In our previous work, we successfully demonstrated the feasibility of a direct nucleophilic ¹⁸F-substitution on *ortho*-halogen-substituted pyridines, following the pioneering study of Dolci et al.^{10,51} The syntheses of the putatively D₃-selective ligands **78** and **79** and the corresponding labeling precursors **84** and **83** were accomplished as illustrated in Scheme 1. Suzuki coupling of 4-carboxybenzene boronic acid with the corresponding bromo-substituted pyridine derivatives **80a–d** was carried out in acetonitrile/water to afford the biarylcarboxylic acids **81a–d** in 43–67% yield. The primary amine **82** was obtained starting from the commercially available 2-methoxyphenylpiperazine by *N*-alkylation with 4-bromobutylphthalimide and subsequent hydrazinolysis.³⁹ The fluoro-substituted lead compounds **78** and **79** and the labeling precursors **83** and **84** were synthesized by DCC-promoted coupling of the carboxylic acids **81a–d** with the aminobutyl-substituted arylpiperazine **82**. The carboxamides **78** and **79** were subjected to *in vitro* biological testing and served as authentic reference compounds in analytical radio-HPLC. Compounds **83** and **84** represent precursors for the nucleophilic, aromatic ¹⁸F-for-NO₂[−] and ¹⁸F-for-Br substitution in DMF, providing access to the radiolabeled ligands [¹⁸F]**79** and [¹⁸F]**78**, respectively. Both leaving groups are suited very well for a nucleophilic, aromatic substitution, as shown by 86% decay-corrected radiochemical yield for [¹⁸F]**79** applying ¹⁸F-for-NO₂ substitution and 73%

Table 4. Radiosynthesis and Radiochemical Yields (RCY; [%]) of the PET Ligands [¹⁸F]**78** and [¹⁸F]**79**^a

labeling precursor	position	leaving group	RCY [%]	C log <i>P</i> ^b
83	3	NO ₂ [−]	[¹⁸ F] 79 : 86 ± 5	79 : 3.36
84	2	Br [−]	[¹⁸ F] 78 : 73 ± 2	78 : 3.57

^a 500 μL DMF, 8 μmol precursor (**84** or **83**), 140 °C, n.c.a. [¹⁸F]fluoride (20 MBq), kryptofix 2.2.2, K₂CO₃, and *t* = 20 min. ^b Calculated value using the program C log *P*; Log *P* of the reference **5** was 5.35

for [¹⁸F]**78** by using bromide as a leaving group (Table 4). Both radioligands [¹⁸F]**79** and [¹⁸F]**78** were synthesized in very high radiochemical yields and in high radiochemical purity under the same reaction conditions, thus providing evidence for the accessibility of these two ¹⁸F-labeled PET ligands in sufficient quality.

Biological Testing. Receptor binding experiments were established to evaluate the binding profile of the fluorinated ligands **78** and **79** (Table 5). D₁ receptor affinities were determined utilizing porcine striatal membranes and the D₁ selective radioligand [³H]SCH 23390.⁵² D_{2long}, D_{2short}, D₃, and D₄ receptor affinities were investigated employing the cloned human dopamine receptor subtypes D_{2long}, D_{2short},⁵³ D₃,⁵⁴ and D_{4.4}⁵⁵ stably expressed in Chinese hamster ovary cells (CHO) and the radioligand [³H]spiperone.⁵⁰ For the investigation of affinity to the related serotonergic receptor subtypes 5-HT_{1A} and 5-HT₂, porcine cortex membranes were used together with the selective radioligands [³H]WAY 100635 and [³H]ketanserin for 5-HT_{1A} and 5-HT₂ receptors, respectively.⁵⁶

The data of the radioligand binding studies showed only poor recognition of the D₁ and 5-HT₂ receptor (Table 5). Although both test compounds **78** and **79** revealed high affinities to the subtypes of the D₂ receptor family as well as to 5-HT_{1A} when binding data between 12 nM and 34 nM were measured, the desired D₃ selectivity of potential PET ligands is indicated by *K*_i values of 0.37 nM and 0.45 nM, as determined for **78** and **79**, respectively. Thus, D₃ affinities were excellent and the selectivities over D_{2long}, D_{2short}, D₄, 5-HT_{1A}, and 5-HT₂ for the fluorinated carboxamide **78** and its regioisomer **79** proved to be >40 and >25, respectively.

Conclusion

The 3D-QSSR analysis presented herein makes it possible to relate chemical structures of ligands with their binding selectivity with respect to different subtypes of a target receptor when using the CoMFA or CoMSIA technique. The derived CoMFA models showed high cross-validation correlation coefficient *q*² values of 0.85 and 0.92 for D₃/D₂ and D₃/D₄ selectivity, respectively, while for the CoMSIA models, the *q*² values were 0.86 and 0.91. The high *q*² values, along with further testing, indicate that the obtained QSSR models should be valuable in predicting the selectivity of new ligands. Using a test set of 14 compounds, we evaluated the predictive performance of the models on external ligands, demonstrating their applicability by a mean predictive *r*² of 0.84 (CoMFA) and 0.78 (CoMSIA) for the D₃/D₂ selectivity model and 0.90 (CoMFA) and 0.93 (CoMSIA) for the D₃/D₄ selectivity model, respec-

Table 5. Binding Affinities of the Fluorinated Target Compounds **78** and **79** to the Human Dopamine Receptor Subtypes D_{2long}, D_{2short}, D₃, and D₄, the Porcine D₁ Receptor, and the Porcine 5-HT_{1A} and 5-HT₂^a

cpd	K _i values ± SD in [nM]						
	[³ H]SCH 23390	[³ H]spiperone				[³ H]8-OH-DPAT	[³ H]ketanserin
	D ₁	D _{2long}	D _{2short}	D ₃	D _{4,4}	5-HT _{1A}	5-HT ₂
78	870 ± 14	27 ± 7.1	16 ± 1.4	0.37 ± 0.064	28 ± 3.5	16 ± 1.4	450 ± 28
79	1300 ± 210	15 ± 7.1	12 ± 0.71	0.45 ± 0.0070	34 ± 1.4	21 ± 6.4	760 ± 120

^a K_i values in nM are based on the means of two experiments, each done in triplicate.

tively. This was extended to the successful application of our analyses in guiding the synthesis of novel PET tracers for D₃ receptors, namely, [¹⁸F]**78** and its regioisomer [¹⁸F]**79**, both revealing high subtype selectivity and good binding affinity.

Experimental Section

Structure Generation, Conformational Analysis, and Alignment. Structure building and refinement of the structures **1–79** (Chart 1 and Tables 1 and 3) has been accomplished using SYBYL 6.9 molecular modeling package⁵⁷ running on indigo2 and octane2 Workstations (MIPS R10000 and R12000).

Because the used molecules show high structural diversity, we selected several templates to compile representative conformations for each group: **7**, **22**, **23**, and **25** for heteroarylcarboxamides, **31** for fused heteroaryl- and biarylmethylenes, and **45** for phenyltetrahydropyridines.

Their geometry was optimized by a grid search (Tripos force field,⁵⁸ Gasteiger–Marsili charges),^{59,60} followed by hierarchical clustering to select the most reasonable low-energy conformer. The shape of all the other ligands was deduced from the corresponding templates. The reference structures haloperidol (**48**) and aripiprazole (**49**) were constructed, and their conformational space was evaluated as described for the template structures. Finally all compounds were optimized with MOPAC using the AM1-Hamiltonian^{61,62} (MMOK was used to fix amide bonds). Subsequently, we calculated VESPA charges⁶³ (implemented in VAMP⁶⁴) for all ligands, which then were aligned to template **7** (showing high selectivity for D₃/D₂ and D₃/D₄) using the module ASP⁴⁵ as implemented in the QSAR package TSAR.⁴⁶ One goal of this study was to test the predictability of the analyses and to design and synthesize new PET imaging agents of improved selectivity toward the D₃ receptor. Therefore, we divided the compounds into a training set containing 63 compounds and a test set of 14 compounds to assess the predictive power of the model. These sets contained compounds from all structural families and represented a balanced number of both the more-selective and the less-selective compounds.

CoMFA and CoMSIA. CoMFA was performed using the QSAR module in Sybyl 6.9. The steric and electrostatic potential fields for CoMFA were calculated at each lattice intersection of a regularly spaced grid of 1.0 Å, while the other SYBYL default parameters were used. The grid was setup with boundaries extending 4 Å beyond the van der Waals envelopes of all molecules including a distance-dependent dielectric constant. A sp³ carbon atom with a charge of +1.0 served as the probe atom to calculate steric and electrostatic fields. These contributions were truncated at 30 kcal/mol and scaled by the CoMFA standard option. As first reported by Cho et. al.,⁶⁵ the cross-validated *r*² (*q*²) value, which serves as a quantitative measure of the predictability, fluctuates with the absolute orientation of the aligned molecular aggregate toward the grid. The reason for this fluctuation is the fact that conventional CoMFA samples the continuous molecular field at discrete lattice points and calculates the steric and electrostatic field energies on each lattice point with distance-sensitive functions, such as the Lennard–Jones 6–12 potential. When the molecular aggregate rotates/translates, so does the molecular field surrounding the aggregate. The lattice box in CoMFA, however, is always axis-aligned and does not rotate/translate along with them. Thus, different points in the same molecular field will be mapped onto the lattice points, resulting in different field energy values. These values, when processed subsequently by PLS to produce the final model, will

cause a variation in the *q*² value and, hence, the predictivity of the model. A Sybyl programming language (SPL) script was written and published by Wang et al.⁴⁷ to perform the all orientation search (AOS)/APS routine automatically. We applied the APS routine to address the phenomena of the translational dependence of the CoMFA described before. The five similarity indices in CoMSIA (steric, electrostatic, hydrophobic, H-bond donor, and H-bond acceptor descriptors) were calculated¹⁸ using a probe atom with a radius of 1 Å and a charge of +1.0 placed at the lattice points of the same region box as was used for the conventional CoMFA calculations. A Gaussian-type distance dependence was used between the grid points and each atom of the molecule. The default value of 0.3 was chosen for the attenuation factor (*α*). Here, steric indices are related to the third power of the atomic radii, electrostatic descriptors are derived from atomic partial charges, hydrophobic fields are derived from atom-based parameters,⁶⁶ and H-bond donor and acceptor indices are obtained by a rule-based method based on experimental results.⁶⁷

Partial Least-Squares (PLS) Analysis. The conventional CoMFA and CoMSIA descriptors derived above were utilized as explanatory variables, and the differences Δ*p*K_i = *p*K_i(D₃) – *p*K_i(D_{2/4}) represented the target variable in PLS^{14,68} regression analyses to derive 3D-QSAR models using the implementation in the SYBYL package. The leave-one-out (LOO) algorithm was selected in the crossvalidation run to obtain the optimal number of components, the lowest standard error of prediction and the corresponding *q*² coefficient. Only a subset of CoMFA field sample points showing a standard deviation of ≥2.0 kcal/mol (*σ*_{min} value for column filtering) were taken to perform PLS regression analysis. The cross-validated coefficient, *q*², was calculated using the following equation

$$q^2 = 1 - \frac{\sum (Y_{\text{pred}} - Y_{\text{actual}})^2}{\sum (Y_{\text{actual}} - Y_{\text{mean}})^2}$$

where *Y*_{pred}, *Y*_{actual}, and *Y*_{mean} are the predicted, actual, and mean values of the target property, respectively. Σ(*Y*_{pred} – *Y*_{actual})² results in the predictive sum of squares (PRESS). The number of principal components resulting in the lowest PRESS value (the optimal number of components (ONC)) was included in the generation of the final non-crossvalidated PLS model,⁶⁹ which yielded the final correlation coefficient *r*² and its standard error *s*. CoMFA and CoMSIA coefficient maps were generated by interpolation of the pairwise products between the PLS coefficients and the standard deviations of the corresponding CoMFA or CoMSIA descriptor values.

General Procedure for the Preparation of Pyridinyl Benzoic Acids **81a–d via Suzuki Reaction.**⁷⁰ To a solution of *p*-carboxybenzene boronic acid (1 mmol) and bromopyridine (1 mmol) in 0.4 M sodium carbonate solution (5 mL) and acetonitrile (5 mL) was added Pd(PPh₃)₄ (60 mg, 0.05 mmol). The mixture was stirred at 90 °C for 3 h. After filtration of the hot suspension, the filtrate was concentrated under reduced pressure to about half of the volume. The concentrate was washed with CH₂Cl₂, and the separated aqueous layer was acidified with HCl (32%). The precipitate was collected, washed with water, and dried on air without purification.

4-(6-Bromopyridin-2-yl)-benzoic Acid (81c**).** Starting from 4-carboxybenzene boronic acid (166 mg, 1 mmol), **80c** (237 mg, 1

mmol), Na₂CO₃ solution (5 mL, 0.4 M), acetonitrile (5 mL), and Pd(PPh₃)₄ (60 mg, 0.05 mmol), **81c** (175 mg, 67%) was obtained as a white solid: ¹H NMR (360 MHz, DMSO-*d*₆) δ 7.7 (d, 1H), 7.85 (t, 1H), 8.08 (d, 2H), 8.11 (d, 1H), 8.18 (d, 2H), 13.1 (m, 1H).

General Procedure for the Carboxamide Synthesis via DCC Coupling. 4-(4-(2-Methoxyphenyl)piperazin-1-yl)butylamine (**82**) was prepared in two steps from 1-(2-methoxyphenyl)piperazine and bromobutylphthalimide, followed by cleaving the phthalimide with hydrazine.³⁹ To a solution of the amine **82** (1 equiv) in dry CH₂Cl₂ (15 mL) was added DMAP (1.25 equiv) and the corresponding carboxylic acids **81a–d** (1 equiv) under an argon atmosphere. To this solution DCC (1.25 equiv) was added. The mixture was stirred at room temperature overnight. The precipitate was removed, and the solution was washed with water (2 × 20 mL) and brine (20 mL). After separation, the organic layer was dried with Na₂SO₄ and concentrated under reduced pressure. The residue was purified by column chromatography over silica gel using CH₂Cl₂/MeOH (9:1) to give **78**, **79**, **83**, and **84** in chemical purity >95%.

N-[4-[4-(2-Methoxyphenyl)piperazin-1-yl]butyl]-4-(6-bromopyridin-2-yl)benzamide (84). According to the general procedure for the DCC coupling, 4-[4-(2-methoxyphenyl)-piperazin-1-yl]butylamine (119 mg, 0.45 mmol), DMAP (74 mg, 0.6 mmol), and **81c** (125 mg, 0.45 mmol) were stirred in 15 mL CH₂Cl₂. After adding dicyclohexylcarbodiimide (124 mg, 0.6 mmol), **84** (172 mg, 73%) was obtained as a white solid: ¹H NMR (360 MHz, CDCl₃) δ 1.55 (m, 4H), 2.36 (t, 2H), 2.49 (m, 4H), 2.94 (s, 4H), 3.29 (m, 2H), 3.74 (s, 3H), 6.84 (m, 4H), 7.59 (d, 1H), 7.81 (t, 1H), 7.93 (d, 2H), 8.06 (m, 3H), 8.48 (t, 1H); APCI-MS *m/z* 524.46 (M⁺, 100).

N-[4-[4-(2-Methoxyphenyl)piperazin-1-yl]butyl]-4-(6-fluoropyridin-2-yl)benzamide (78). According to the general procedure for the DCC coupling 4-[4-(2-methoxyphenyl)-piperazin-1-yl]butylamine (105 mg, 0.4 mmol), DMAP (61.1 mg, 0.5 mmol), and **81d** (87 mg, 0.4 mmol) were stirred in 15 mL CH₂Cl₂. After adding dicyclohexylcarbodiimide (103 mg, 0.5 mmol), **78** (120 mg, 65%) was obtained as a white solid: ¹H NMR (360 MHz, CDCl₃) δ 1.7 (m, 4H), 2.55 (t, 2H), 2.73 (s, 4H), 3.08 (m, 4H), 3.51 (q, 2H), 3.86 (s, 3H), 6.87 (m, 4H), 6.98 (m, 1H), 7.07 (dd, 1H), 7.64 (m, 1H), 7.88 (m, 3H), 8.06 (m, 2H); APCI-MS *m/z* 463.56 (M⁺, 100). Anal. (C₂₇H₃₁FN₄O₂): C, H, N.

Radiosyntheses of N-[4-[4-(2-Methoxyphenyl)piperazin-1-yl]butyl]-4-(6-[¹⁸F]fluoropyridin-2-yl)benzamide (¹⁸F)78** and N-[4-[4-(2-Methoxyphenyl)piperazin-1-yl]butyl]-4-(6-[¹⁸F]fluoropyridin-3-yl)benzamide (¹⁸F)**79**.** No-carrier-added [¹⁸F]fluoride was produced by the ¹⁸O(p,n)¹⁸F reaction using a RDS 111 cyclotron (CTI) at PET Net GmbH (Erlangen, Germany). A QMA-cartridge with [¹⁸F]fluoride (typically 300 MBq) was eluted with a solution of 15 mg Kryptofix 2.2.2/15 μL of 1 N potassium carbonate stock solution in 1 mL acetonitrile/water (8:2). The solvent was evaporated by azeotropic drying under a stream of nitrogen at 85 °C. This procedure was repeated two times using 500 μL of acetonitrile. The dry residue was resolubilized with a solution of 8 μmol of precursor **84** or **83** in 500 μL of dry DMF. Samples of the solution (25 μL) were isolated in periods of 5, 10, 20, and 30 min. These samples were used for determination of radiochemical yields by reversed-phase HPLC. The identification of radiofluorinated PET ligands [¹⁸F]**78** and [¹⁸F]**79** was performed by reversed-phase radio HPLC (RP 18 Select B5 column (250 × 4 mm) eluted with acetonitrile/water (70:30, 0.1% TFA, 1 mL/min)) using the UV absorbance at 254 nm of the standard compounds **78** (*t_R* = 14.6 min) and **79** (*t_R* = 12.5 min) as a reference signal. Analytical HPLC was performed on the following system: HPLC Hewlett-Packard (HP 1100) with a quaternary pump and variable wavelength detector (HP 1100) connected to a radio-HPLC detector D505TR (Canberra Packard). Computer analysis of the HPLC data was performed using FLO-One software (Canberra Packard).

Receptor Binding Experiments. Receptor binding studies were carried out as described in the literature.⁵² In brief, the dopamine D₁ receptor assay was done with porcine striatal membranes at a final protein concentration of 40 μg/assay tube and the radioligand [³H]SCH 23390 at 0.3 nM (*K_d* = 0.65 nM). Competition experi-

ments with the human D_{2long}, D_{2short}, D₃ and D_{4.4} receptors were run with preparations of membranes from CHO cells expressing the corresponding receptor and [³H]spiperone at a final concentration of 0.1 nM (for D₄ at 0.2 nM). The assays were carried out with a protein concentration of 1.5–8 μg/assay tube and *K_d* values of 0.05 nM for D_{2long}, 0.03 nM for D_{2short}, 0.08 nM for D₃, and 0.16 nM for D_{4.4}. The investigation of serotonin 5-HT_{1A} and 5-HT₂ binding was performed as described in the literature.⁵⁶ In brief, porcine cortical membranes were subjected to the binding assay at a concentration of 55 μg/assay tube and 100 μg/assay tube for determination of 5-HT_{1A} and 5-HT₂ binding utilizing [³H]WAY 100–635 and [³H]ketanserin each at a final concentration of 0.1 nM and 0.5 nM, respectively, and with *K_D* values of 0.07 nM (for 5-HT_{1A}) and 1.5 nM (for 5-HT₂). Protein concentration was established by the method of Lowry using bovine serum albumin as standard.⁷¹ Data analysis of the resulting competition curves was accomplished by nonlinear regression analysis using the algorithms in PRISM (GraphPad software, San Diego, CA). *K_i* values were derived from the corresponding EC₅₀ data utilizing the equation of Cheng and Prusoff.⁷²

Acknowledgment. This work was supported by the DFG (Pr 677/2). I. Salama wishes to thank the Egyptian government for the long-term scholarship. The authors wish to thank Dr. J.-C. Schwartz, Dr. P. Sokoloff (INSERM, Paris), and the Institute of Psychiatry, Toronto, as well as J. Shine (The Garvan Institute of Medical Research, Sydney) for providing dopamine D₄, D₃, and D₂ receptor expressing cell lines, respectively.

Supporting Information Available: Figures showing contour maps of D₃/D₂ and D₃/D₄ selectivity models as obtained by CoMFA and CoMSIA analyses, methods and materials, preparation/analytical data of **79**, **81a,b,d**, and **83**, and a table of elemental analysis data. This material is available free of charge via the Internet at <http://pubs.acs.org>.

References

- Massoud, T. F.; Gambhir, S. S. Molecular imaging in living subjects: Seeing fundamental biological processes in a new light. *Genes Dev.* **2003**, *17*, 545–580.
- Lemaire, C.; Damhaut, P.; Plenevaux, A.; Comar, D. Enantioselective synthesis of 6-[fluorine-18]-fluoro-L-dopa from no-carrier-added fluorine-18-fluoride. *J. Nucl. Med.* **1994**, *35*, 1996–2002.
- Langer, O.; Nagren, K.; Dollé, F.; Lundkvist, C.; Sandell, J.; Swahn, C.-G.; Vaufrey, F.; Crouzel, C.; Maziere, B.; Halldin, C. Precursor synthesis and radiolabelling of the dopamine D-2 receptor ligand [C-11]raclopride from [C-11]methyl triflate. *J. Labelled Compd. Radiopharm.* **1999**, *42*, 1183–1193.
- Mukherjee, J.; Christian, B. T.; Dunigan, K. A.; Shi, B.; Narayanan, T. K.; Satter, M.; Mantil, J. Brain imaging of ¹⁸F-fallypride in normal volunteers: Blood analysis, distribution, test–retest studies, and preliminary assessment of sensitivity to aging effects on dopamine D-2/D-3 receptors. *Synapse* **2002**, *46*, 170–188.
- Boeckler, F.; Gmeiner, P. The structural evolution of dopamine D3 receptor ligands: Structure–activity relationships and selected neuropharmacological aspects. *Pharmacol. Ther.* **2006**, *112*, 281–333.
- Langer, O.; Gulyas, B.; Sandell, J.; Laszlovszky, I.; Kiss, B.; Domany, G.; ACS, T.; Farde, L.; Halldin, C. Radiochemical labelling of the dopamine D-3 receptor ligand RGH-1756. *J. Labelled Compd. Radiopharm.* **2000**, *43*, 1069–1074.
- Sovago, J.; Farde, L.; Halldin, C.; Langer, O.; Laszlovszky, I.; Kiss, B.; Gulyas, B. Positron emission tomographic evaluation of the putative dopamine-D3 receptor ligand, [¹¹C]RGH-1756 the monkey brain. *Neurochem. Int.* **2004**, *45*, 609–617.
- De Vries, E. F.; Kortekaas, R.; van Waarde, A.; Dijkstra, D.; Elsinga, P. H.; Vaalburg, W. Synthesis and evaluation of dopamine D3 receptor antagonist 11C-GR218231 as PET tracer for P-glycoprotein. *J. Nucl. Med.* **2005**, *46*, 1384–1392.
- Seeman, P.; Wilson, A.; Gmeiner, P.; Kapur, S. Dopamine D2 and D3 receptors in human putamen, caudate nucleus, and globus pallidus. *Synapse* **2006**, *60*, 205–211.
- Hocke, C.; Prante, O.; Löber, S.; Hübner, H.; Gmeiner, P.; Kuwert, T. Synthesis and evaluation of ¹⁸F-labeled dopamine D3 receptor ligands as potential PET imaging agents. *Bioorg. Med. Chem. Lett.* **2005**, *15*, 4819–4823.

- (11) Lanig, H.; Utz, W.; Gmeiner, P. Comparative molecular field analysis of dopamine D4 receptor antagonists including 3-[4-(4-chlorophenyl)-piperazin-1-ylmethyl]pyrazolo[1,5-*a*]pyridine (FAUC 113), 3-[4-(4-chlorophenyl)piperazin-1-ylmethyl]-1*H*-pyrrolo-[2,3-*b*]pyridine (L-745,870), and clozapine. *J. Med. Chem.* **2001**, *44*, 1151–1157.
- (12) Boeckler, F.; Ohnmacht, U.; Lehmann, T.; Utz, W.; Hübner, H.; Gmeiner, P. CoMFA and CoMSIA investigations revealing novel insights into the binding modes of dopamine D3 receptor agonists. *J. Med. Chem.* **2005**, *48*, 2493–2508.
- (13) Salama, I.; Schlotter, K.; Utz, W.; Hübner, H.; Gmeiner, P.; Boeckler, F. CoMFA and CoMSIA investigations of dopamine D3 receptor ligands leading to the prediction, synthesis, and evaluation of rigidized FAUC 365 analogues. *Bioorg. Med. Chem.* **2006**, *14*, 5898–5912.
- (14) Cramer, R. D., III; Patterson, D. E.; Bunce, J. D. Comparative molecular field analysis (CoMFA). 1. Effect of shape on binding of steroids to carrier proteins. *J. Am. Chem. Soc.* **1988**, *110*, 5959–5967.
- (15) Kubinyi, H., Ed. *3D-QSAR in Drug Design. Theory, Methods and Applications*; ESCOM: Leiden, The Netherlands, 1993.
- (16) Kubinyi, H.; Folkers, G.; Martin, Y. C., Eds. *3D-QSAR in Drug Design. Volume 2. Ligand–Protein Interactions and Molecular Similarity*; Kluwer/ESCOM: Dordrecht, The Netherlands, 1997.
- (17) Kubinyi, H.; Folkers, G.; Martin, Y. C., Eds. *3D-QSAR in Drug Design. Volume 3. Recent Advances*; Kluwer/ESCOM: Dordrecht, The Netherlands, 1998.
- (18) Klebe, G.; Abraham, U.; Mietzner, T. Molecular similarity indices in a comparative analysis (CoMSIA) of drug molecules to correlate and predict their biological activity. *J. Med. Chem.* **1994**, *37*, 4130–4146.
- (19) Böhm, M.; Stürzebecher, J.; Klebe, G. Three-dimensional quantitative structure–activity relationship analyses using comparative molecular field analysis and comparative molecular similarity indices analysis to elucidate selectivity differences of inhibitors binding to trypsin, thrombin, and factor Xa. *J. Med. Chem.* **1999**, *42*, 458–477.
- (20) Baskin, I. I.; Tikhonova, I. G.; Palyulin, V. A.; Zefirov, N. S. Selectivity fields: Comparative molecular field analysis (CoMFA) of the glycine/NMDA and AMPA receptors. *J. Med. Chem.* **2003**, *46*, 4063–4069.
- (21) Yang, G.-F.; Lu, H.-T.; Xiong, Y.; Zhan, C.-G. Understanding the structure–activity and structure–selectivity correlation of cyclic guanidine derivatives as phosphodiesterase-5 inhibitors by molecular docking, CoMFA and CoMSIA analyses. *Bioorg. Med. Chem.* **2006**, *14*, 1462–1473.
- (22) Melville, J. L.; Lovelock, K. R. J.; Wilson, C.; Allbutt, B.; Burke, E. K.; Lygo, B.; Hirst, J. D. Exploring phase-transfer catalysis with molecular dynamics and 3D/4D quantitative structure selectivity relationships. *J. Chem. Inf. Model.* **2005**, *45*, 971–981.
- (23) Catto, M.; Nicolotti, O.; Leonetti, F.; Carotti, A.; Favia, A. D.; Soto-Otero, R.; Mendez-Alvarez, E.; Carotti, A. Structural insights into monoamine oxidase inhibitory potency and selectivity of 7-substituted coumarins from ligand- and target-based approaches. *J. Med. Chem.* **2006**, *49*, 4912–4925.
- (24) Mach, R. H.; Hammond, P. S.; Huang, Y.; Yang, B.; Xu, Y.; Cheney, J. T.; Freeman, R.; Luedtke, R. R. Structure–activity relationship studies of *N*-(9-benzyl)-9-azabicyclo[3.3.1]nonan-3- β -yl benzamide analogues for dopamine D₂ and D₃ receptors. *Med. Chem. Res.* **1999**, *9*, 355–373.
- (25) Wilcox, R. E.; Tseng, T.; Brusniak, M. Y.; Ginsburg, B.; Pearlman, R. S.; Teeter, M.; DuRand, C.; Starr, S.; Neve, K. A. CoMFA-based prediction of agonist affinities at recombinant D1 vs D2 dopamine receptors. *J. Med. Chem.* **1998**, *41*, 4385–4399.
- (26) Wilcox, R. E.; Huang, W. H.; Brusniak, M. Y.; Wilcox, D. M.; Pearlman, R. S.; Teeter, M. M.; DuRand, C. J.; Wiens, B. L.; Neve, K. A. CoMFA-based prediction of agonist affinities at recombinant wild type versus serine to alanine point mutated D2 dopamine receptors. *J. Med. Chem.* **2000**, *43*, 3005–3019.
- (27) Ravina, E.; Negreira, J.; Cid, J.; Masaguer, C. F.; Rosa, E.; Rivas, M. E.; Fontenla, J. A.; Loza, M. I.; Tristan, H.; Cadavid, M. I.; Sanz, F.; Lozoya, E.; Carotti, A.; Carrieri, A. Conformationally constrained butyrophenones with mixed dopaminergic (D₂) and serotonergic (5-HT_{2A}), 5-HT_{2C}) affinities: Synthesis, pharmacology, 3D-QSAR, and molecular modeling of (aminoalkyl)benzo- and thienocycloalkanes as putative atypical antipsychotics. *J. Med. Chem.* **1999**, *42*, 2774–2797.
- (28) Norinder, U.; Hogberg, T. A quantitative structure–activity relationship for some dopamine D₂ antagonists of benzamide type. *Acta Pharm. Nord.* **1992**, *4*, 73–78.
- (29) McGaughey, G. B.; Mewshaw, R. E. Application of comparative molecular field analysis to dopamine D₂ partial agonists. *Bioorg. Med. Chem.* **1999**, *7*, 2453–2456.
- (30) Homan, E. J.; Tulp, M. T.; Nilsson, J. E.; Wikström, H. V.; Grol, C. J. C5-substituted derivatives of 5-OMe-BPAT: Synthesis and interactions with dopamine D₂ and serotonin 5-HT_{1A} receptors. *Bioorg. Med. Chem.* **1999**, *7*, 2541–2548.
- (31) Hackling, A.; Ghosh, R.; Perachon, S.; Mann, A.; Höltje, H. D.; Wermuth, C. G.; Schwartz, J. C.; Sippl, W.; Sokoloff, P.; Stark, H. *N*-(ω -(4-(2-Methoxyphenyl)piperazin-1-yl)alkyl)carboxamides as dopamine D₂ and D₃ receptor ligands. *J. Med. Chem.* **2003**, *46*, 3883–3899.
- (32) De Paulis, T.; El Tayar, N.; Carrupt, P. A.; Testa, B.; Van de Waterbeemd, H. Quantitative structure–affinity relationships of dopamine D₂ receptor antagonists: A comparison between orthopramides and 6-methoxysalicylamides. *Helv. Chim. Acta* **1991**, *74*, 241–254.
- (33) Cha, M. Y.; Lee, I. Y.; Cha, J. H.; Choi, K. I.; Cho, Y. S.; Koh, H. Y.; Pae, A. N. QSAR studies on piperazinylalkylisoxazole analogues selectively acting on dopamine D₃ receptor by HQSAR and CoMFA. *Bioorg. Med. Chem.* **2003**, *11*, 1293–1298.
- (34) Boström, J.; Gundertofte, K.; Liljeforsa, T. A pharmacophore model for dopamine D₄ receptor antagonists. *J. Comput.-Aided Mol. Des.* **2000**, *14*, 769–786.
- (35) Boström, J.; Böhm, M.; Gundertofte, K.; Klebe, G. A 3D QSAR study on a set of dopamine D₄ receptor antagonists. *J. Chem. Inf. Comput. Sci.* **2003**, *43*, 1020–1027.
- (36) Löber, S.; Hübner, H.; Gmeiner, P. Azaindole derivatives with high affinity for the dopamine D₄ receptor: Synthesis, ligand binding studies, and comparison of molecular electrostatic potential maps. *Bioorg. Med. Chem. Lett.* **1999**, *9*, 97–102.
- (37) Löber, S.; Hübner, H.; Utz, W.; Gmeiner, P. Rationally based efficacy tuning of selective dopamine D₄ receptor ligands leading to the complete antagonist 2-[4-(4-chlorophenyl)piperazin-1-ylmethyl]pyrazolo[1,5-*a*]pyridine (FAUC 213). *J. Med. Chem.* **2001**, *44*, 2691–2694.
- (38) Löber, S.; Aboul-Fadl, T.; Hübner, H.; Gmeiner, P. Di- and trisubstituted pyrazolo[1,5-*a*]pyridine derivatives: Synthesis, dopamine receptor binding and ligand efficacy. *Bioorg. Med. Chem. Lett.* **2002**, *12*, 633–636.
- (39) Bettinetti, L.; Schlotter, K.; Hübner, H.; Gmeiner, P. Interactive SAR studies: Rational discovery of super-potent and highly selective dopamine D₃ receptor antagonists and partial agonists. *J. Med. Chem.* **2002**, *45*, 4594–4597.
- (40) Bettinetti, L.; Löber, S.; Hübner, H.; Gmeiner, P. Parallel synthesis and biological screening of dopamine receptor ligands taking advantage of a click chemistry based BAL linker. *J. Comb. Chem.* **2005**, *7*, 309–316.
- (41) Loaiza, P. R.; Löber, S.; Hübner, H.; Gmeiner, P. Click chemistry on solid phase: Parallel synthesis of *N*-benzyltriazole carboxamides as super-potent G-protein coupled receptor ligands. *J. Comb. Chem.* **2006**, *8*, 252–261.
- (42) Löber, S.; Hübner, H.; Gmeiner, P. Synthesis and biological investigations of dopaminergic partial agonists preferentially recognizing the D₄ receptor subtype. *Bioorg. Med. Chem. Lett.* **2006**, *16*, 2955–2959.
- (43) Koob, G. F.; Caine, S. B. Cocaine addiction therapy—are we partially there? *Nat. Med.* **1999**, *5*, 993–995.
- (44) Chavez-Eng, C. M.; Constanzer, M. L.; Matuszewski, B. K. Picogram determination of a novel dopamine D₄ receptor antagonist in human plasma and urine by liquid chromatography with atmospheric pressure chemical ionization tandem mass spectrometry. *J. Chromatogr., B.* **1997**, *691*, 77–85.
- (45) ASP V3.22, Oxford Molecular, Ltd.: The Medawar Centre, Oxford Science Park, Sandford-on-Thames, Oxford OX4 4GA, U.K., 1998.
- (46) TSAR V3.2, Oxford Molecular, Ltd.: The Medawar Centre, Oxford Science Park, Sandford-on-Thames, Oxford OX44GA, U.K., 1998.
- (47) Wang, R.; Gao, Y.; Liu, L.; Lai, L. All-orientation search and all-placement search in comparative molecular field analysis. *J. Mol. Model.* **1998**, *4*, 276–283.
- (48) Thibaut, U.; Folkers, G.; Klebe, G.; Kubinyi, H.; Merz, A.; Rognan, D. Recommendations to CoMFA studies and 3D QSAR publications. In *3D QSAR in Drug Design. Theory, Methods and Applications*; Kubinyi, H., Ed.; ESCOM: Leiden, The Netherlands, 1993; pp 711–716.
- (49) Murray, P. J.; Harrison, L. A.; Johnson, M. R.; Robertson, G. M.; Scopes, D. I.; Bull, D. R.; Graham, E.; Hayes, A. G.; Kilpatrick, G. J. A novel series of arylpiperazines with high affinity and selectivity for the dopamine D₃ receptor. *Bioorg. Med. Chem. Lett.* **1995**, *5*, 219–222.
- (50) Yuan, Y.; Chen, C.; Brodbeck, R.; Primus, R.; Braun, J.; Wasley, J. W. F.; Thurkauf, A. NGB 2904 and NGB 2849: Two highly selective dopamine D₃ receptor antagonists. *Bioorg. Med. Chem. Lett.* **1998**, *8*, 2718–2718.
- (51) Dolci, L.; Dollé, F.; Jubeau, S.; Vaufrey, F.; Crouzel, C. 2-[¹⁸F]-fluoropyridines by no-carrier-added nucleophilic aromatic substitution with [¹⁸F]FK-K₂₂₂—a comparative study. *J. Labelled Compd. Radiopharm.* **1999**, *42*, 975–985.

- (52) Hübner, H.; Haubmann, C.; Utz, W.; Gmeiner, P. Conjugated enynes as nonaromatic catechol bioisosteres: Synthesis, binding experiments, and computational studies of novel dopamine receptor agonists recognizing preferentially the D3 subtype. *J. Med. Chem.* **2000**, *43*, 756–762.
- (53) Hayes, G.; Biden, T. J.; Selbie, L. A.; Shine, J. Structural subtypes of the dopamine D2 receptor are functionally distinct: expression of the cloned D2A and D2B subtypes in a heterologous cell line. *Mol. Endocrinol.* **1992**, *6*, 920–926.
- (54) Sokoloff, P.; Andrieux, M.; Besançon, R.; Pilon, C.; Martres, M.-P.; Giros, B.; Schwartz, J.-C. Pharmacology of human dopamine D3 receptor expressed in a mammalian cell line: Comparison with D2 receptor. *Eur. J. Pharmacol.* **1992**, *225*, 331–337.
- (55) Asghari, V.; Sanyal, S.; Buchwaldt, S.; Paterson, A.; Jovanovic, V.; Van Tol, H. H. M. Modulation of intracellular cyclic AMP levels by different human dopamine D4 receptor variants. *J. Neurochem.* **1995**, *65*, 1157–1165.
- (56) Schlotter, K.; Boeckler, F.; Hübner, H.; Gmeiner, P. Fancy bioisosteres: Metallocene-derived G-protein-coupled receptor ligands with subnanomolar binding affinity and novel selectivity profiles. *J. Med. Chem.* **2005**, *48*, 3696–3699.
- (57) Sybyl 6.9, Tripos, Inc.: 1699 South Hanley Road, St. Louis, Missouri, 63144, 2002.
- (58) Clark, M.; Cramer, R.-D.; Van Opdenbosch, N. Validation of the general purpose Tripos 5.2 force field. *J. Comput. Chem.* **1989**, *10*, 982–1012.
- (59) Gasteiger, J.; Marsili, M. Iterative partial equalization of orbital electronegativity: A rapid access to atomic charges. *Tetrahedron* **1980**, *36*, 3219–3222.
- (60) Hinze, J.; Jaffe, H. H. Electronegativity. I. Orbital electronegativity of neutral atoms. *J. Am. Chem. Soc.* **1962**, *84*, 540–546.
- (61) Stewart, J. J. MOPAC: A semiempirical molecular orbital program. *J. Comput.-Aided Mol. Design* **1990**, *4*, 1–105.
- (62) Stewart, J. J. P.; Frank, J. MOPAC; Seiler Bokstav Research Laboratory: United States Air Force Academy, CO 80840, 1990.
- (63) Beck, B.; Clark, T.; Glen, R. C. A detailed study of VESPA electrostatic potential-derived atomic charges. *J. Mol. Model.* **1995**, *1*, 176–187.
- (64) Clark, T.; Alex, A.; Beck, B.; Chandrasekar, J.; Gedeck, P.; Horn, A.; Huttern, M.; Martin, B.; Rauhut, G.; Sauer, W.; Schindler, T.; Steinke, T. *VAMP 7.0 Program Package*; Oxford Molecular Plc.: Oxford, 1998.
- (65) Cho, S. J.; Tropsha, A. Cross-validated R²-guided region selection for comparative molecular field analysis: A simple method to achieve consistent results. *J. Med. Chem.* **1995**, *38*, 1060–1066.
- (66) Viswanadhan, V. N.; Ghose, A. K.; Revankar, G. R.; Robins, R. K. Atomic physicochemical parameters for three dimensional structure directed quantitative structure-activity relationships. 4. Additional parameters for hydrophobic and dispersive interactions and their application for an automated superposition of certain naturally occurring nucleoside antibiotics. *J. Chem. Inf. Comput. Sci.* **1989**, *29*, 163–172.
- (67) Klebe, G. The use of composite crystal-field environments in molecular recognition and the de novo design of protein ligands. *J. Mol. Biol.* **1994**, *237*, 212–235.
- (68) Wold, S. Validation of QSAR's. *Quant. Struct.-Act. Relat.* **1991**, *10*, 191–193.
- (69) Baroni, M.; Clementi, S.; Cruciani, G.; Costantino, G.; Riganeli, D.; Oberrauch, E. Predictive ability of regression models. Part II. Selection of the best predictive PLS model. *J. Chemom.* **1992**, *6*, 347–356.
- (70) Gong, Y.; Pauls, H. W. A convenient synthesis of heteroaryl benzoic acids via suzuki reaction. *Synlett* **2000**, *6*, 829–831.
- (71) Lowry, O. H.; Rosebrough, N. J.; Farr, A. L.; Randall, R. J. Protein measurement with the folin phenol reagent. *J. Biol. Chem.* **1951**, *193*, 265–275.
- (72) Cheng, Y. C.; Prusoff, W. H. Relationship between the inhibition constant (K_i) and the concentration of inhibitor which causes 50% inhibition (IC_{50}) of an enzymatic reaction. *Biochem. Pharmacol.* **1973**, *22*, 3099–3108.

JM0611152